

This is the preprint of the contribution published as:

Klöckner, P., Seiwert, B., Weyrauch, S., Escher, B.I., Reemtsma, T., Wagner, S. (2021):
Comprehensive characterization of tire and road wear particles in highway tunnel road dust by
use of size and density fractionation
Chemosphere **279** , art. 130530

The publisher's version is available at:

<http://dx.doi.org/10.1016/j.chemosphere.2021.130530>

1 **Comprehensive characterization of tire and road wear particles in highway tunnel road**
2 **dust by use of size and density fractionation**

3
4 Philipp Klöckner ^a, Bettina Seiwert ^a, Steffen Weyrauch ^a, Beate I. Escher ^{b,c}, Thorsten
5 Reemtsma ^{a,d}, Stephan Wagner ^a

6
7 ^a Helmholtz-Centre for Environmental Research – UFZ, Department Analytical Chemistry,
8 Permoserstr. 15, 04318 Leipzig, Germany

9 ^b Helmholtz-Centre for Environmental Research – UFZ, Department Cell Toxicology,
10 Permoserstr. 15, 04318 Leipzig, Germany

11 ^c Eberhard-Karls-University Tübingen, Center for Applied Geoscience, Environmental
12 Toxicology, Schnarrenbergstr. 94-96, 72076 Tübingen, Germany

13 ^c University of Leipzig, Institute of Analytical Chemistry, Linnéstrasse 3, 04103, Leipzig,
14 Germany

15
16 Corresponding author: thorsten.reemtsma@ufz.de

17
18 **Key words:** TWP, microplastics, PM10, air pollution, runoff

19
20

21
22
23
24
25
26
27
28
29
30
31
32
33
34
35
36
37
38

CRedit author statements:

Philipp Klöckner: Formal analysis; Investigation; Methodology; Visualization; Writing - original draft; Writing - review & editing. **Bettina Seiwert:** Formal analysis; Investigation; Methodology. **Steffen Weyrauch:** Formal analysis; Investigation. **Beate Escher:** Formal analysis; Investigation; Methodology; Writing - review & editing. **Thorsten Reemtsma:** Funding acquisition; Project administration; Resources; Writing - review & editing. **Stephan Wagner:** Conceptualization; Resources; Supervision; Writing - review & editing.

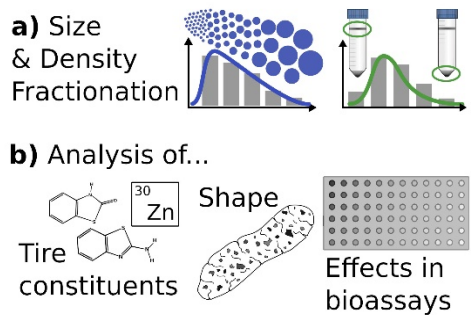
Highlights:

- Tire and road wear particles (TRWPs) in tunnel dust: smaller and less dense than in road simulators.
- Mass distributions of tire constituents had maxima in the size fraction < 20 µm.
- Density of TRWPs was mostly in the range of 1.3 - 1.7 g/cm³.
- Elongated particles were identified in size and density fractions.
- Solvent extracts of tunnel dust activated oxidative stress response in bioassays.

Graphical abstract:



TRWPs in tunnel dust



39

41 Abstract

42 Tire and road wear particles (TRWPs) are generated by abrasion of vehicle tires and
43 agglomeration with particles from the road surface. Even though they constitute a major
44 component of particulate non-exhaust traffic emissions, knowledge about their physico-
45 chemical properties is limited and largely based on road simulator experiments. Tunnel road
46 dust was analyzed for TRWPs and their sizes, densities and shapes. Solvent extracts were
47 characterized for presence of seven tire tread indicator chemicals and their effects in *in vitro*
48 bioassays.

49 The peak of the TRWP mass distribution was in the size fraction 20 - 50 μm , with 31 - 36%
50 of the total TRWP mass and a content of up to 260 mg/g. The mass of organic tire
51 constituents peaked in the smallest analyzed size fractions ($< 20 \mu\text{m}$) with 35 - 55% of their
52 total mass. Density of TRWPs in tunnel dust was 1.3 - 1.7 g/cm^3 , which was lower than
53 expected. Video-based shape analysis and SEM showed elongated particles, likely TRWP, to
54 be present in those size and density fractions ascribed to TRWPs by chemical analysis.
55 However, also irregular heteroagglomerates that may be TRWPs could be found.
56 Solvent extracts of size and density fractions induced effects in bioassays indicative of the
57 activation of the arylhydrocarbon receptor (AhR-CALUX) and the adaptive response to
58 oxidative stress (AREC32) that exceeded previously reported mixture effects of extracts from
59 river sediments.

60 Similar comprehensive characterization of road dust at other sites may help increase the
61 knowledge about physico-chemical properties of TRWPs. If the properties of TRWPs in
62 tunnels and on open roads are similar, tunnel dust would be a promising basis for preparation
63 of test materials because of its comparably high TRWP content and less environmental
64 influence.

65 1. Introduction

66 The abrasion of vehicle tires releases high amounts of tire and road wear particles (TRWPs).
67 These TRWPs are heteroagglomerates of tread rubber, road material and particles deposited
68 on the road (Kreider et al., 2010; Wagner et al., 2018), whereas particles of “pure” tire tread
69 would be described as tire particles (TPs). Due to the uncertainties about TRWP composition,
70 emission estimates usually provide values in TP/a, such as for example 75,000 - 130,000 t
71 TP/a in Germany (Baensch-Baltruschat et al., 2021; Kole et al., 2017; Wagner et al., 2018).
72 Particles encrusted in the rubber matrix of TRWPs may be for example mineral grains,
73 bitumen or other particulate traffic emissions (Adachi and Tainosho, 2004; Kreider et al.,
74 2010; Sommer et al., 2018). Data on TRWP properties are scattered and often difficult to
75 compare due to differences in analysis techniques, generation conditions or experimental
76 setups (Grigoratos and Martini, 2014). For example, variable degrees of encrusted particles in
77 TRWPs in the range of 10 - 50 % have been reported (Kreider et al., 2010; Sommer et al.,
78 2018; Unice et al., 2019a). Most studies characterized TRWPs from road simulators
79 (Grigoratos and Martini, 2014; Wagner et al., 2018) instead of environmental TRWPs.
80 Especially the size distribution of TRWPs in environmental samples in the range of 10 - 1000
81 μm is poorly studied (Wagner et al., 2018), and hardly any measured data on the density of
82 TRWPs is available (Klöckner et al., 2020, 2019).
83 TRWPs have been described as having an elongated shape (Adachi and Tainosho, 2004;
84 Kovoichich et al., 2021; Kreider et al., 2010; Sommer et al., 2018), while fine TRWPs (0.001
85 - 10 μm) that are generated by volatilization and subsequent condensation are rather spherical
86 or irregular (Dahl et al., 2006; Kim and Lee, 2018).

87 More reliable data on physicochemical properties are of great importance as input parameters
88 for particle transport models. Providing these data requires validated analytical workflows
89 and representative samples.

90 It was assumed, that road dust collected in tunnels may have higher contents of TRWPs than
91 dust collected from open roads, because there are fewer particle sources and no precipitation.
92 TRWPs in tunnel dust may also be less aged due to absence of sunlight and rainfall. Tunnel
93 dust or TRWPs isolated from it may therefore be suitable as test materials for the
94 development of analytical methods and for experimental purposes, for aging and leaching
95 studies and testing of biological effects.

96 The content of TRWPs may be determined by quantification of marker compounds, such as
97 thermal degradation products of styrene-butadiene rubber, benzothiazole derivatives or
98 hydrogenated resin acids (Wagner et al., 2018). Particulate Zn in the density fraction <1.9
99 g/cm^3 (TRWP_{Zn}) was suggested as a marker for TRWPs (Klößner et al., 2019). Organic tire
100 constituents, such as 2-hydroxybenzothiazole (OHBT) and 2-aminobenzothiazole (ABT),
101 may also be indicators of TRWP contents in street dust (Klößner et al., 2020). If chemical
102 analyses are combined with physical fractionation methods, particle properties may be
103 derived.

104 Tire rubber toxicity was previously related to heavy metals or organic compounds, such as
105 benzothiazole derivatives, aromatic amines or phthalates (Wagner et al., 2018) and recently
106 to a transformation product of the antiozonant N-(1,3-dimethylbutyl)-N'-phenyl-1,4-
107 phenylenediamine (6PPD) leaching from tires, 6-PPD-quinone (Tian et al., 2020). Tire-
108 associated chemicals, such as benzothiazole-2-sulfonic acid (BTSA) and OHBT have been
109 shown to reach high concentrations in street-runoff (Kloepfer et al., 2005) and in urban rivers
110 after strong rainfall, together with 1,3-diphenylguanidine (DPG), and hexamethoxymethyl
111 melamine (Seiwert et al., 2020). BTSA was shown to be a major effect driver for the
112 activation of the arylhydrocarbon receptor (AhR) and the oxidative stress response in rivers
113 during rainfall events (Neale et al., 2020). These findings emphasize the need for toxicity
114 testing of TRWPs and their constituents.

115 A comprehensive characterization of TRWPs in tunnel road dust with complementary
116 techniques was performed in this study, aiming to (i) obtain data on the size, density and
117 shape of TRWPs in tunnel dust samples, (ii) determine cytotoxicity and specific effects in
118 bioassays of size and density fractions of tunnel dust, and (iii) compare this data set with
119 existing data of environmental and road simulator samples. The presented workflow may be a
120 basis for future TRWP research and the production of TRWP test materials.

121

122 2. Materials and Methods

123

123 2.1. Sampling and sample preparation

124 Samples A and B were obtained on 21st January 2020 in the tunnel "Königshainer Berge" at
125 highway A4 in the direction to Görlitz (Germany; 51°12'53.2"N, 14°48'42.8"E). The tunnel
126 has a length of 3300 m, separate tubes for each direction and a speed limit of 80 km/h.

127 Sampling was performed in the middle (A) and the last quarter (B) of the tunnel (after 1680
128 m and 2760 m), using a pressure washer and a wet vacuum cleaner (NT 45/1 Tact, Kärcher,
129 Winnenden, Germany). The right lane was sampled including the sidewalk. Samples were
130 transferred into sealed buckets and stored in the laboratory over night at room temperature.

131 Water was removed by centrifugation (Rotanta 460, 2500 rpm, 10 min, rcf = 1360 x g,
132 Hettich, Tuttlingen, Germany). The supernatant was decanted and settled particles were
133 rinsed out with ultrapure water (Milli-Q integral, Merck KGaA, Darmstadt, Germany). The
134 samples were frozen (-18 °C), freeze-dried and dry sieved to a size of < 1 mm.

135 **2.2. Size fractionation**

136 50 g subsamples were sieved using a vibratory sieve shaker (AS200, Retsch, Haan,
137 Germany), tap water, and sieves with mesh sizes of 20, 50, 100, 250 and 500 μm . Particles
138 were rinsed off the sieves with ultrapure water, frozen (-18 °C) and freeze-dried. Particles
139 <20 μm were collected in a bucket and centrifuged (Section 2.1). The mass recovery in size
140 fractionation was 98.0% (sample A) and 97.5% (sample B).

141 **2.3. Density fractionation**

142 Subsamples (ca. 2 g) were added to 50 mL tubes (Nunc, Thermo Scientific, Waltham USA)
143 and 45 mL sodium polytungstate solution (SPT; TC-Tungsten Compounds, Grub am Forst,
144 Germany) of variable concentration/density (see below) were added. Samples were vortexed
145 (2000 rpm, 10 min, Reax 2000, Heidolph Instruments, Schwabach, Germany), centrifuged
146 (Rotanta 460, 3000 rpm, 10 min, rcf = 1950 x g), and the buoyant fraction was decanted. The
147 process was repeated with 12 mL SPT solution of the same density before the next highest
148 density was added. Densities of SPT solution were 1.3, 1.5, 1.7, 1.9, 2.1, and 2.3 g/cm^3 . The
149 fractions were filtered onto 0.8 μm cellulose nitrate membrane filters (Labsolute, Th. Geyer,
150 Renningen, Germany). The mass recovery in density fractionation was 97% (sample A) and
151 92% (sample B).

152 **2.4. Microwave digestion and elemental analysis**

153 A subsample of approx. 500 mg of the dried samples was digested in 6 mL nitric acid (HNO_3 ,
154 Chemsolute, superpure grade, 67-70%, Th. Geyer, Renningen, Germany) and 2 mL hydrogen
155 peroxide (H_2O_2 , Suprapur, 30%, Merck, Darmstadt, Germany) using a microwave digestion
156 system (Multiwave, Anton Paar, Graz, Austria; $T_{\text{max}} = 260$ °C; $p_{\text{max}} = 60$ bar). For density
157 fractions < 500 mg, the whole fraction was digested. Elemental analysis of diluted digests
158 was performed using inductively coupled plasma mass spectrometry (ICP-MS; iCAP Q S,
159 Thermo Scientific, Waltham, USA). Measurement conditions can be found in Table S1.

160 **2.5. TRWP_{Zn} determination**

161 TRWPs quantified by analysis of particulate Zn in the density fraction <1.9 g/cm^3 (Klößner
162 et al., 2020) are denoted as TRWP_{Zn} . In short, density separation of dried dust (approx. 1 g)
163 using SPT solution of density 1.9 g/cm^3 was performed after vortexing and treatment in an
164 ultrasonic bath for particle dispersion. The buoyant fraction was filtered, rinsed, dried and
165 analyzed for Zn after digestion. TRWP_{Zn} content was initially calculated assuming a content
166 of 4.35 mg Zn/g TRWP based on a Zn content in TP of 8.7 mg/g and 50% TP content
167 (Klößner et al., 2019). However, results of density fractionation (Section 3.3) indicated that
168 in the present samples, a TP content of 75% in TRWPs was more appropriate, and the
169 calculation of TRWP_{Zn} was adjusted, accordingly.

170 **2.6. Organic extraction**

171 Dried subsamples (50 mg or less) were added to glass vial (n=3). 5 mL methanol (MeOH,
172 Suprasolv grade, Merck, Darmstadt, Germany) were added and extraction was performed for
173 1 h in an ultrasonic bath (Sonorex Digitec DT 255 H, Bandelin instruments, Berlin,
174 Germany). Overlaying solvent was transferred into a syringe (Braun Injekt Solo, 5 mL, B.
175 Braun, Melsungen, Germany), filtered through a 0.22 μm PTFE syringe filter (Membrane
176 solutions, Plano, Texas, USA) into a 2 mL screw neck vial (ND8, Labsolute, Th. Geyer,
177 Renningen, Germany) and diluted with ultrapure water to a final concentration of 50% (v/v)
178 methanol.

179 2.7. UPLC-ToF-MS analysis

180 MeOH extracts were analyzed with ultra-performance liquid chromatography time-of-flight
181 mass spectrometry (UPLC-ToF-MS). The instrumental setup consisted of an ACQUITY
182 UPLC-System (HSS T3 column, 100 × 2.1 mm, 1.7 μm) and a XEVO XS Q-TOF-MS
183 (Waters GmbH, Eschborn, Germany). Instrumental parameters can be found in Table S2.
184 TargetLynx was used for quantitative analysis and exact mass accuracy had to be < 5 ppm.
185 The seven analytes OHBT, ABT, 6PPD, OBS (2-(4-morpholinyl)benzothiazole), BT
186 (benzothiazole), aniline and DPG, were quantified by external quantification (Table S3).
187 Two compounds were determined by their exact masses and fragmentation products: 6PPD-Q
188 (Tian et al., 2020; Fig. S1) and a formylated transformation product of 6PPD, with an exact
189 mass of 297.1964 (positive ionization mode) and a retention time of 10.7 min (“marker
190 297”). This compound showed a high aging resistance and low leaching potential and
191 occurred in different tire treads (data not shown).
192 For each analyte, the content (C) in one size or density fraction (F) was calculated from the
193 mass of the analyte in the respective fraction (m_{analyte}) and the respective fraction mass
194 (m_{fraction} ; Equation 1).

$$195 \quad C(F) = \frac{m_{\text{analyte}}}{m_{\text{fraction}}} \quad (1)$$

196 For each analyte, the mass percentage (M) in a size or density fraction (F) was calculated
197 from m_{analyte} and the total analyte mass ($m_{\text{a,total}}$) as shown in Equation 2. The total analyte
198 mass was calculated as the sum of m_{analyte} of all fractions.

$$199 \quad M(F) = \frac{m_{\text{analyte}}}{m_{\text{a,total}}} * 100 \quad (2)$$

199

200 2.8. Shape analysis

201 Subsamples (ca 1. mg, n=3) were dispersed in 4 mL of 2-propanol (ULC-MS - CC/SFC
202 grade, Bisolve Chimie, Dieuze, France) by a magnetic stirring unit (ACM-101; 12600 rpm).
203 The minimum measuring time in video-based dynamic image analysis (EyeTech Combi, EW
204 lens, Ambivalue, Dussen, Netherlands) was 60 s and the minimum particle number was 500.
205 The average of two measuring cycles was formed. The circularity was calculated by the
206 projection area (A) and the perimeter (P) of a particle (Equation 3).

$$207 \quad \text{Circularity} = \frac{A * 4\pi}{P^2} \quad (3)$$

208 The number of particles in classes with a width of 0.05 was calculated. Scaling was
209 performed to the highest frequency of each replicate.

210 2.9. SEM imaging

211 Samples were applied on stubs for scanning electron microscopy (SEM; Merlin VP Compact,
212 Carl Zeiss, Oberkochen, Germany) using conductive adhesive tape (Plano, Wetzlar,
213 Germany). Samples were sputter-coated with chromium (EM SCD 500, Leica Microsystems,
214 Wetzlar, Germany). Instrumental parameters are listed in Table S4.

215 2.10. *In vitro* bioassays

216 MeOH extracts of sample B (n=3) were used for two mammalian reporter gene assays:
217 AREc32 (Wang et al., 2006) and AhR-CALUX (chemical activated luciferase gene
218 expression; cell line H4L7.5c2; Brennan et al., 2015). Cells were seeded in 384-well plates in
219 30 μl of assay medium and incubated (37°C, 5% CO₂, 95% humidity) for 24 h (König et al.,
220 2017; Neale et al., 2017). 10 μl of sample were added to each well and incubation continued

221 for 24 h. The samples were a dilution series with duplicates of each concentration of
222 reference chemicals and extract dissolved in assay medium. Cell viability was calculated
223 using cell confluency detected by an IncuCyte S3 live cell imaging system (Essen
224 BioScience, Ann Arbor, Michigan, USA). The inhibitory concentration for 10% reduction of
225 cell viability (IC₁₀) was determined from the linear range of the concentration-response
226 curve. Concentrations above the IC₁₀ were excluded.
227 Luciferase activity was measured as luminescence after addition of cell lysis buffer and
228 incubation for 10 min at RT followed by addition of 20 µl of luciferase substrate buffer. The
229 relative light units (RLU) were converted to induction ratios (IR) for AREc32. The effect
230 concentration causing an IR of 1.5 (EC_{IR1.5}) was deduced from a linear concentration-
231 response model up to IR 4 (Escher et al., 2018). For AhR, the RLU of the unexposed cells
232 was set to 0% and the maximum RLU induced by 2,3,7,8-tetrachlorodibenzodioxin (TCDD)
233 to 100%. All RLU were converted to % effect. The effect concentration triggering 10%
234 activation for AhR (EC₁₀) was derived from a linear concentration-response model (Escher et
235 al., 2018).
236 Effect concentrations of a sample EC_{sample} were translated to bioanalytical equivalent
237 concentrations BEQ by Equation 4 using the EC_{reference compound} of a reference compound
238 (Escher et al., 2018). This assures that a higher numerical value is associated to a higher
239 effect.

$$240 \quad \text{BEQ} = \frac{\text{EC}_{\text{reference compound}}}{\text{EC}_{\text{sample}}} \quad (4)$$

241 Reference compounds were t-butylhydroquinone (tBHQ) for AREc32 and TCDD for AhR
242 CALUX. The BEQ are called tBHQ-EQ and TCDD-EQ. The EC were converted using an
243 EC₁₀ of 0.207±0.005 ng_{TCDD}/L_{bioassay} (Fig. S7a) and EC_{IR1.5} of 450±10 µg_{tBHQ}/L_{bioassay} (Fig.
244 S7b).
245

246 3. Results & Discussion

247 3.1. Characterization of tunnel dust samples < 1 mm

248 The two samples of tunnel dust (A, B) had mostly similar properties (Table 1, Table S5,
249 Table S6). For TRWP_{Zn}, a 50% content of TP in TRWPs was assumed previously (Klößner
250 et al., 2019), but in the present samples, the TP content was approximately 75% (Section 3.3).
251 The TRWP_{Zn} quantification was adjusted, accordingly. The TRWP_{Zn} content of 110 - 120
252 mg/g was more than one order of magnitude higher than previous findings in road dust
253 (Klößner et al., 2020), which may confirm the expected “purity” of tunnel dust.
254 Analogously, much higher values of OHBT (factor 10) and ABT (factor 3-4) were found than
255 in street dust outside of tunnels (Asheim et al., 2019; Klößner et al., 2020; Zhang et al.,
256 2018).

257
258
259

Table 1: Content of selected organic tire constituents, Zn and TRWP_{Zn} as well as mean particle density and mode of circularity in the two tunnel samples. One standard deviation is indicated by \pm . Values were rounded to two significant digits. TRWP_{Zn} contents were provided based on 50%* and 75% TP in TRWP, respectively.**

Analyte / Property	Unit	Sample A	Sample B
6PPD	ng/mg	1.5 \pm 0.044	1.9 \pm 0.14
OHBT	ng/mg	1.3 \pm 0.0075	1.5 \pm 0.2
ABT	ng/mg	0.12 \pm 0.0022	0.13 \pm 0.0094
Marker 297	peak area / mg	45 \pm 1.9	55 \pm 6.6
6PPD-Q	peak area / mg	220 \pm 9.5	270 \pm 27
Zn	mg/g	2.0 \pm 0.15	2.1 \pm 0.54
TRWP_{Zn}	mg/g	170* / 110**	180* / 120**
Particle density	g/cm ³	2.2	2.1
Particle shape	Circularity	0.62 \pm 0.34	0.62 \pm 0.43

260

261 Differences could be observed for the particle size distributions of the two samples (Fig. 1a):
262 Sample A had a higher share of fine particles < 20 μm (32% by mass) while coarser particles
263 > 250 μm were larger in sample B (44%).

264 The size distribution of road dust may vary with local conditions such as pavement type,
265 climatic conditions, driving speed or the surrounding environment. The fraction of road dust
266 < 100 μm in other studies was approximately between 10 - 30% by mass if an upper particle
267 size cutoff of 1 mm was considered (Adachi and Tainosho, 2005; Han et al., 2008; Klöckner
268 et al., 2020; Polukarova et al., 2020; Wang et al., 2005; Zafra et al., 2011). Accordingly, the
269 two samples of tunnel dust are composed of finer particles, which may be due to fewer
270 secondary particle sources inside the tunnel.

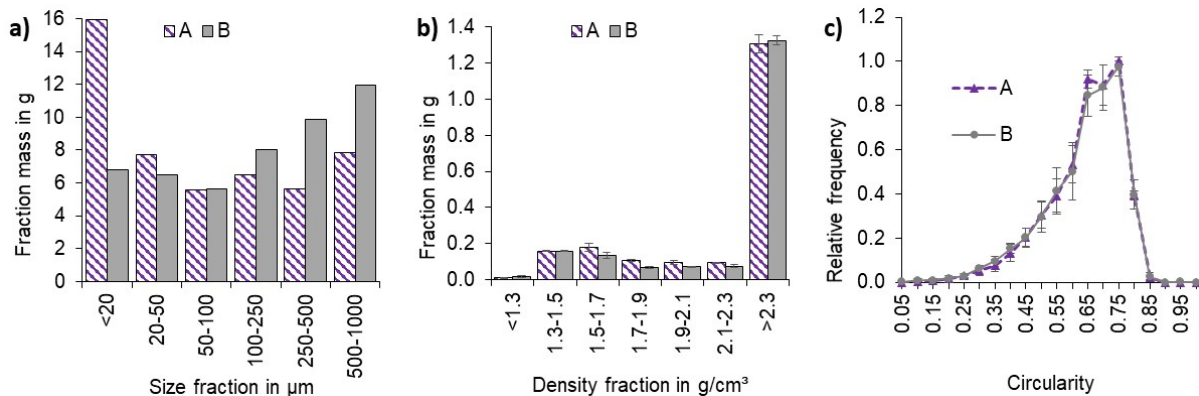
271 The mean particle density of the two tunnel samples agreed well to values reported for road
272 dust with a low amount of organic detritus (2.1 - 2.5 g/cm³; Zanders, 2005) and is at the
273 upper end of other data for road dust (1.5 - 2.5 g/cm³, Kayhanian et al., 2012; Zanders, 2005).

274 This corresponds to the expected reduced influence of organic matter inside the tunnel.

275 The density distribution of particulate matter was similar in both samples (Fig. 1b): it is
276 dominated by the fraction > 2.3 g/cm³ (mineral matter; approximately 65% by mass),
277 whereas the fraction < 1.3 g/cm³ (organic matter) was practically absent (0.5 - 1% by mass).
278 The four density fractions in the range 1.5 - 2.3 g/cm³ had approximately equal masses and
279 each contributed between 3.4% and 8.9% to the total sample mass.

280 Also, particle shapes, as shown by their circularity, were similar in both samples (Fig. 1c).

281 Spherical particles (circularity = 1) and particles of very low circularity (e.g. fibers,
282 circularity approaches 0) were absent. Both distributions were skewed towards higher
283 circularities. The mode of the particle circularity (Table 1) indicated a low to moderate
284 circularity (Blott and Pye, 2008), i.e. slightly elongated particles. This was lower than road
285 dust and TRWPs in a previous study, where circularities of 0.83 - 0.84 were determined
286 (Kreider et al., 2010).



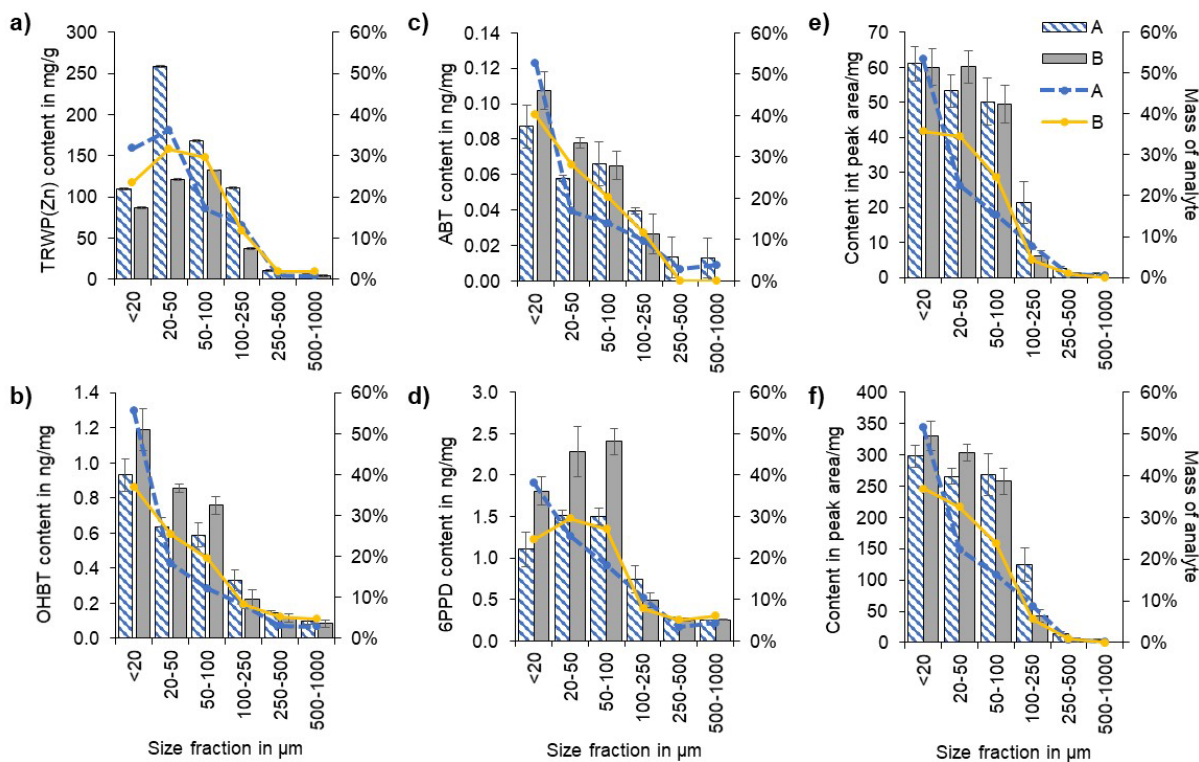
287
 288 **Figure 1: a) Masses of size fractions of the two tunnel road dust samples A and B as obtained by wet-sieving. b)**
 289 **Masses of density fractions as obtained by density separation. Error bars show one standard deviation. c) Circularity**
 290 **of particles as determined by video analysis in both samples, scaled to the highest particle count of each replicate.**
 291

292 3.2. TRWPs in size fractions

293 The size of TRWPs is one of the major determinants of their fate in the environment
 294 (Besseling et al., 2017; Unice et al., 2019b). In the tunnel dust, the content of organic tire
 295 constituents (OHBT, ABT, 6PPD) increased from the coarser (500 - 1000 μm) to the finer
 296 fractions (<math>< 50 \mu\text{m}</math>) by a factor of about 5 - 10 (Fig. 2 b, c, d). For 6-PPDQ, a compound
 297 recently identified as being toxic to fish (Tian et al., 2020), and marker 297, the contents even
 298 increased by a factor of 50 - 80 (Fig. 2e, f). For TRWP_{Zn}, the highest contents (120 - 260
 299 mg/g) occurred in the size range 20 - 50 μm or 50 - 100 μm rather than in the finest fraction
 300 of the tunnel dust, but this trend remains scattered, as for 6-PPD (Fig. 2a, d). With 12 - 26%
 301 of weight, TRWPs were highly concentrated in the size fractions 20 - 50 μm and 50 - 100 μm
 302 of tunnel dust.

303 The masses of organic compounds and TRWP_{Zn} throughout the size fractions were not evenly
 304 distributed (Fig. 2, lines). While above 250 μm , organic compounds and TRWP_{Zn} were
 305 practically absent, their mass increased towards the smallest size fraction by a factor of 5
 306 (6PPD) to 70 (marker 297). For both samples, the masses of OHBT, ABT, 6PPD-Q and
 307 marker 297 were highest in the size fraction <math>< 20 \mu\text{m}</math> (approx. 35 - 55%), while TRWP_{Zn}
 308 peaked in the fraction 20 - 50 μm (approx. 30 - 35%). The particle size distribution of
 309 TRWPs therefore appeared to have a mode in the smallest size fractions (Fig. S2).

310 Studies reporting size distributions of TRWPs in particle size ranges 10 - 1000 μm are scarce.
 311 A road simulator study determined TRWP size distributions to range from 5 - 220 μm with a
 312 mode at 75 μm (determined by laser diffraction) or 4 - 350 μm with a mode at 100 μm
 313 (determined by optical microscopy; Kreider et al., 2010). Recently, the volume size
 314 distribution of TRWPs from a road simulator was reported between 6 μm and 120 μm , with a
 315 mean of 49 μm (Kovochich et al., 2021). TRWPs from road dust collected by sweeper cars
 316 were mainly > 50 μm in size (Klöckner et al., 2020) but may have been affected by size-
 317 dependent sweeping efficacy, whereas in the present study pressure washing was applied.
 318 The present data is, thus, showing a distribution with finer particle sizes than expected. It is
 319 not clear whether this is due to the tunnel situation, collection on a highway with higher
 320 driving speed or to other factors, including techniques of particle collection.



322
 323 **Figure 2: a) TRWP_{Zn} b) OHBT, c) ABT, d) 6PPD and e) marker 297, f) 6PPD-Q in size fractions of tunnel**
 324 **road dust (samples A, B). Columns: content in mg/g, ng/mg, or peak area/mg (Eq. 1; left y-axis). Error**
 325 **bars show one standard deviation (n=3). Lines: mass of an analyte in a fraction in % of the total mass of**
 326 **the analyte (Eq. 2, right y-axis). TRWP_{Zn} was calculated based on 75% TP content in TRWPs.**

327 3.3. TRWPs in density fractions

328 Not only the size, but also the density of TRWPs is relevant for their transport in the
 329 environment, since it affects the settling velocity in water and, thus, their travel distance
 330 (Besseling et al., 2017; Unice et al., 2019b).

331 Tunnel dust was fractionated into seven density fractions from < 1.3 to > 2.3 g/cm³, followed
 332 by chemical analysis of the fractions. The contents of the organic tire constituents and Zn
 333 increased with decreasing density (Fig. 3, Fig. S4). In the fractions < 1.7 g/cm³, contents were
 334 up to 4x higher than in the fractions > 1.7 g/cm³.

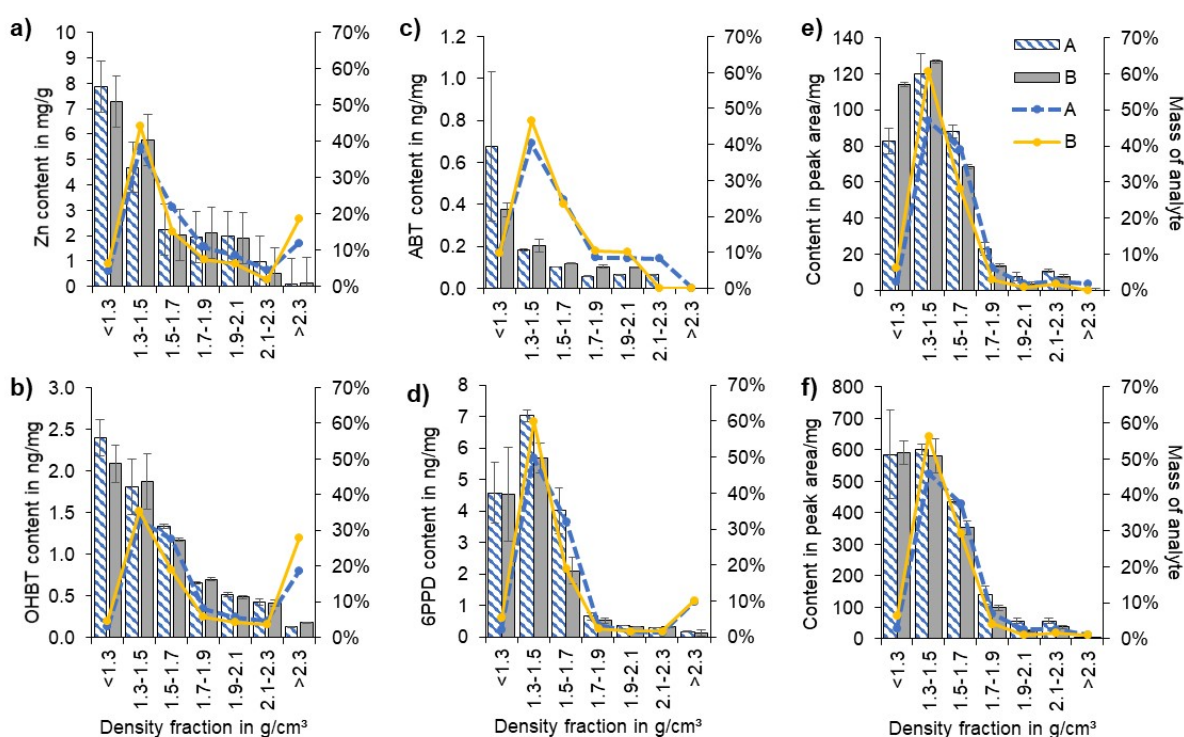
335 The mass distribution of all organic tire constituents and Zn over the density fractions
 336 consistently show a maximum of TRWPs in the density fractions 1.3 - 1.7 g/cm³ (Fig. 3,
 337 lines). Assuming a density of 1.2 g/cm³ for tire tread (Degaffe and Turner, 2011), this would
 338 correspond to a mass contribution of encrusted particles in the present TRWPs of around 25%
 339 (TRWP density of 1.5 g/cm³). TRWP_{Zn} contents based on the Zn content in TP and an
 340 assumed content of 50% TP would therefore overestimate the TRWP content in the present
 341 samples and the quantification of TRWP_{Zn} was based on 75% TP in TRWP, accordingly.

342 The density of TRWPs was in previous studies inferred from the proportion of encrusted
 343 minerals (Kreider et al., 2010), resulting in a density estimate of 1.8 g/cm³ for TRWPs from a
 344 road simulator (50% mineral contribution; Unice et al., 2019a). The discrepancy with TRWP
 345 densities estimated in the present study, may either be due to fewer non-tire particles present
 346 in TRWP or due to a lower density of such encrusted particles than in previous estimates
 347 (Kreider et al., 2010). Sommer et al (2018) reported that highway TRWPs contained only 6 -
 348 10 % vol of encrusted particles and calculated a total density of 1.26 g/cm³. This agrees well
 349 to the samples of this study. Analyses of road dust from urban roads indicated that 73 - 98%

350 of TRWPs had a density $< 1.9 \text{ g/cm}^3$ (Klößner et al., 2020), whereas in sediments of settling
 351 ponds for runoff, densities were occasionally $> 1.9 \text{ g/cm}^3$ (Klößner et al., 2020).
 352 Sample processing may in the present study have led to the loss of encrusted particles from
 353 TRWPs during sampling or sample processing. The stability of TRWP agglomerates has not
 354 been studied so far.

355 Distributions similar to the organic tire constituents and Zn were obtained for Sb and Sn,
 356 while As, Ba, Bi, Cd, Co, Cu, Cr, and Pb were clearly dominant in the fraction $> 2.3 \text{ g/cm}^3$ (;
 357 Fig. S5). Of these, Ba, Co, Cu, Cr, and Pb have been used as marker elements for brake wear
 358 emissions (Grigoratos and Martini, 2014) or asphalt wear (Mummullage et al., 2016), which
 359 agrees to their presence in the high density fraction. While Sb and Sn are also associated with
 360 brake wear particles (Grigoratos and Martini, 2014) they are present also in TPs (Klößner et
 361 al., 2019; Kreider et al., 2010; Sommer et al., 2018). In these samples of tunnel dust, TPs may
 362 be the predominant source of these two elements.

363



364
 365 **Figure 3:** a) Zn, b) OHBT, c) ABT, d) 6PPD, e) marker 297 and f) 6PPD-Q in density fractions of tunnel dust samples
 366 (A, B). Columns: content of the analytes in each density fraction in mg/g, ng/mg or peak area/mg (Eq. 1, left y-axis).
 367 Error bars show one standard deviation (n=3). ABT was not detected in the density fraction $> 2.1 \text{ g/cm}^3$ (sample B)
 368 and $> 2.3 \text{ g/cm}^3$ (both samples). Lines: mass of an analyte in a fraction in % of the total mass of the analyte (Eq. 2,
 369 right y-axis). Please note that TRWP_{Zn} is not shown because it is defined as particulate Zn in the density fraction $<$
 370 1.9 g/cm^3 .

371

372 3.4. Shape analysis and SEM imaging

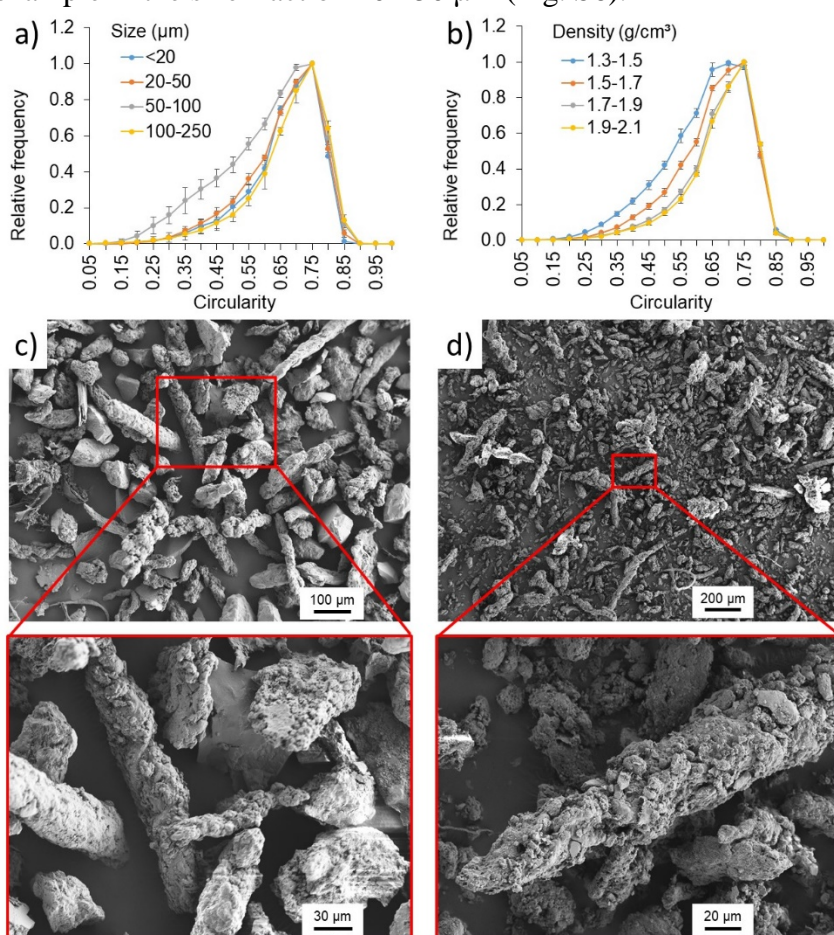
373 Since TRWPs have been described as sausage-shaped particles in previous studies, selected
 374 fractions of sample B were analyzed for their circularity (Fig. 4a, b). The fraction $< 1.3 \text{ g/cm}^3$
 375 could not be analyzed in sample B due to limitations in material availability, which is why a
 376 subsample of sample A was used here.

377 Concerning the size fractions, a higher frequency of elongated particles was visible in the
 378 fraction 50 - 100 μm (Fig. 4a). While a high content of TRWP would be expected in this
 379 fraction based on chemical analysis, the same would be true for the size fractions $< 20 \mu\text{m}$

380 and 20 - 50 μm (Fig. 2). These fractions, however, did not show a higher frequency of
381 elongated particles, suggesting that in these smallest size fractions not all TRWPs are
382 elongated.

383 Concerning the density, elongated particles were most frequent in the two fractions between
384 1.3 - 1.7 g/cm^3 (Fig. 4b). The shape analysis from the density fractions, thus, agreed well with
385 the results from the organic tire constituents and Zn (Fig. 3).

386 In the size and density fractions with higher abundance of elongated particles, characteristic
387 TRWPs could be identified by SEM imaging (Fig. 4c, d). These particles matched the shapes
388 and agglomerate compositions of TRWPs of earlier studies (Kreider et al., 2010; Sommer et
389 al., 2018). In accordance to the lower density of TRWP in the tunnel dust (Section 3.3), the
390 number of encrusted particles visible from the SEM pictures appeared to be lower than on
391 pictures shown in previous studies (Kreider et al., 2010; Sommer et al., 2018). Apart from
392 elongated particles, also irregular particles with encrustations could be observed in SEM, for
393 example in the size fraction 20 - 50 μm (Fig. S6).

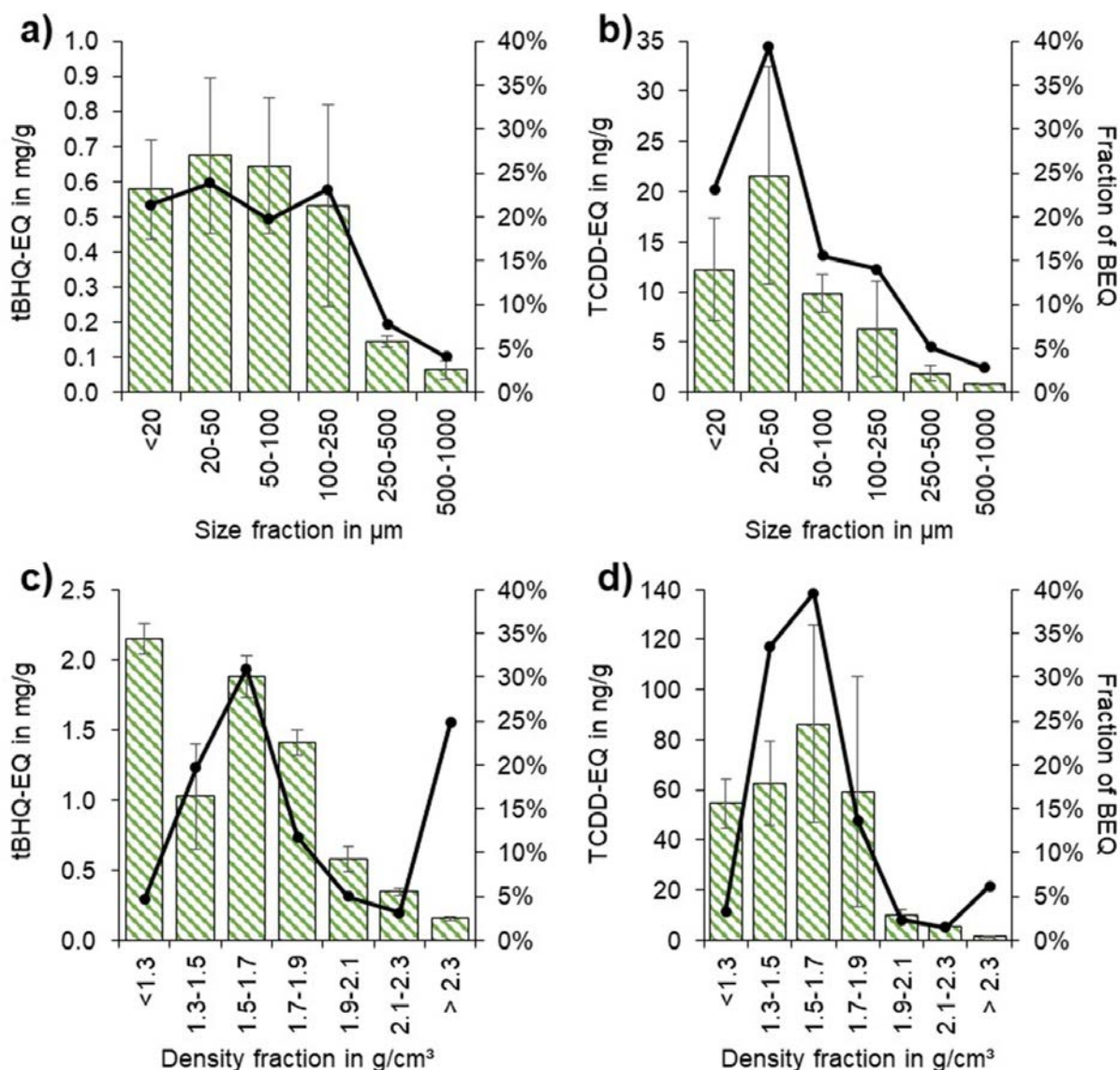


394
395 **Figure 4:** Circularity of particles as determined by video-based shape analysis of four different size fractions (a) and
396 four different density fractions (b) of sample B. Density fraction 1.3 - 1.5 g/cm^3 was analyzed in a subsample of
397 sample A due to limited sample availability after density separation. The data was scaled to the highest particle count
398 of each fraction for better comparability. SEM images of the size fraction 50 - 100 μm (c) and density fractions 1.3 -
399 1.5 g/cm^3 (d) of sample B and enlarged details thereof.
400

401 3.5. *In vitro* bioassays

402 The effect screening of methanol extracts of sample B and its size and density fractions
403 aimed at complementing the above characterization with integrate measures of overall
404 cytotoxicity and specific modes of action that were previously shown to be relevant for road
405 runoff (Neale et al., 2020). For AREc32, no cytotoxicity was observed up to an enrichment of

406 4 g_{particles}/L_{bioassay}, while the AhR CALUX cell line was more sensitive and cytotoxicity was
407 detected in most extracts (Fig. S7, Table S7). The IC₁₀ ranged from 65 to >1000
408 mg_{particles}/L_{bioassay} (Table S7). Despite the low cytotoxicity, all samples activated AhR and the
409 oxidative stress response, with no responses in procedural blanks (Table S7). Effects were
410 stronger in AhR CALUX cells, with EC up to two orders of magnitude lower than on the
411 AREc32. The effect concentrations of the triplicate extracts were averaged and they showed
412 large variability (CV 6% to 77%, Table S8) was presumably due to the heterogeneity of the
413 particles, since CV of individual extracts were typically below 10% (Table S7). Effect
414 concentrations translated to BEQ (tBHQ-EQ and TCDD-EQ; Table S8), were by a factor 2 to
415 8 higher than for example in river sediment of the Saar (Jahnke et al., 2018), a river highly
416 influenced by contamination with persistent organic pollutants, even though the Saar
417 sediments were extracted with a harsher method (accelerated solvent extraction).
418 For the size fractions, the tBHQ-EQ showed no clear differences between the fractions < 250
419 μm (Fig. 5a). This contrasts with the contents of organic tire constituents (Fig. 2), which were
420 2 - 10 times higher in the fractions < 100 μm compared to the fraction 100 - 250 μm. TCDD-
421 EQ (Fig. 5b) showed the same dependence on size fraction as the contents of TRWP_{Zn} and
422 6PPD.
423 Regarding the density fractions, BEQ (Fig. 5c, d) in the fractions < 1.9 g/cm³ were an order
424 of magnitude higher than in the fractions > 1.9 g/cm³ (factor 14 - 39). Contrary to the organic
425 tire constituents, BEQ from both bioassays in the density fraction 1.7 - 1.9 g/cm³ were
426 comparably high.
427 As for the above analytes, distributions of BEQ were calculated from the BEQ in each
428 fraction relative to the sum BEQ (Fig. 5, lines). The distribution of tBHQ-EQ clearly differed
429 from above mass distributions of organic tire constituents and TRWP_{Zn} in the size fractions
430 but showed a similar distribution for the density fractions. For TCDD-EQ, the distributions in
431 size and density fractions agreed well with the above results, even though minor deviations
432 could be observed in the size fraction < 20 μm or the density fraction 1.7 - 1.9 g/cm³.
433 Effects were, thus, not exclusively associated to TRWP presence, which is no surprise given
434 the number of compounds able to activate AhR or induce oxidative stress. Polycyclic
435 aromatic hydrocarbons, for example, are strong activators of AhR and might be associated to
436 larger soot particles, but are also important TP contaminants (Wagner et al., 2018). The
437 results nonetheless suggest that TRWPs were a major contributor to the observed mixture
438 effects.



439
 440 **Figure 5: BEQ from the two bioassays in size and density fractions. a) tBHQ-EQ in size fractions, b) TCDD-EQ in**
 441 **size fractions, c) tBHQ-EQ in density fractions, d) TCDD-EQ in density fractions. Columns: content of BEQ in mg/g**
 442 **(tBHQ-EQ) and ng/g (TCDD-EQ) in size or density fractions (Eq. 4, left y-axis). Lines: Percentage of BEQ in a size or**
 443 **density fraction relative to the total mass of BEQ (Eq. 2, right y-axis).**
 444

445 **4. Conclusions**

446 Road dust from a highway tunnel was found to contain high TRWP contents of up to 120
 447 mg/g.

448 The highest share of TRWPs (according to Zn and organic indicators) was found in the
 449 density fractions 1.3 - 1.7 g/cm³ and in the size range < 50 µm. In the most concentrated
 450 fraction, the TRWP content reached up to 260 mg/g.

451 TRWPs in the tunnel dust were finer and of lower density than previous reports for TRWP
 452 collected on streets or from road simulators. Different properties of materials from tire test
 453 facilities must be carefully considered when providing test materials and protocols in the
 454 future.

455 Activation of xenobiotic metabolism and oxidative stress response pathways by extracts of
 456 the size and density fractions followed the pattern of the chemical contents, which suggests
 457 that TRWPs contributed to mixture effects in the present sample.

458 Further measurements of real-world TRWPs from different sites are required to learn more
459 about the variable quality of TRWP. It may then be concluded if TRWPs from road tunnels
460 are suited as representative test materials. The workflow applied in this study, consisting of
461 physical fractionation methods and chemical analyses, appears to be well suitable for a
462 comprehensive characterization of TRWP properties.
463

464 5. Acknowledgement

465 The authors thank Christopher Paul (Autobahnmeisterei Weißenberg) for help in sample
466 acquisition. Furthermore, we thank Jan Beck, Daniel Kolb and Jürgen Steffen for help in
467 sample preparation, Josephine Karte for instrumental analysis, Matthias Schmidt for help in
468 preparation of SEM images, Maria König for performance of the bioassays and Rita
469 Schlichting for reviewing the manuscript (all UFZ). The partial funding by the Federal
470 Ministry of Education and Research Germany (BMBF; reference number 02WRS1378H,
471 funding measure RiSKWa) of the project MiWa (“Microplastic in the water cycle - sampling,
472 sample treatment, analysis, occurrence, elimination and assessment”) is acknowledged
473 gratefully. This research was also supported by the Helmholtz Research Program “Terrestrial
474 Environment”, Topic 3: “Sustainable Water Resources Management”. We gratefully
475 acknowledge access to the platform CITEPro (Chemicals in the Terrestrial Environment
476 Profiler) funded by the Helmholtz Association.
477

478 6. References

- 479 Adachi, K., Tainosho, Y., 2005. Single particle characterization of size-fractionated road
480 sediments. *Appl. Geochemistry* 20, 849–859.
481 <https://doi.org/10.1016/j.apgeochem.2005.01.005>
- 482 Adachi, K., Tainosho, Y., 2004. Characterization of heavy metal particles embedded in tire
483 dust. *Environ. Int.* 30, 1009–1017. <https://doi.org/10.1016/j.envint.2004.04.004>
- 484 Asheim, J., Vike-Jonas, K., Gonzalez, S. V., Lierhagen, S., Venkatraman, V., Veivåg, I.L.S.,
485 Snilsberg, B., Flaten, T.P., Asimakopoulos, A.G., 2019. Benzotriazoles, benzothiazoles
486 and trace elements in an urban road setting in Trondheim, Norway: Re-visiting the
487 chemical markers of traffic pollution. *Sci. Total Environ.* 649, 703–711.
488 <https://doi.org/10.1016/j.scitotenv.2018.08.299>
- 489 Baensch-Baltruschat, B., Kocher, B., Kochleus, C., Stock, F., Reifferscheid, G., 2021. Tyre
490 and road wear particles - A calculation of generation, transport and release to water and
491 soil with special regard to German roads. *Sci. Total Environ.* 752, 141939.
492 <https://doi.org/10.1016/j.scitotenv.2020.141939>
- 493 Besseling, E., Quik, J.T.K., Sun, M., Koelmans, A.A., 2017. Fate of nano- and microplastic
494 in freshwater systems: A modeling study. *Environ. Pollut.* 220, 540–548.
495 <https://doi.org/10.1016/j.envpol.2016.10.001>
- 496 Blott, S.J., Pye, K., 2008. Particle shape: A review and new methods of characterization and
497 classification. *Sedimentology* 55, 31–63. <https://doi.org/10.1111/j.1365-3091.2007.00892.x>
- 499 Brennan, J.C., He, G., Tsutsumi, T., Zhao, J., Wirth, E., Fulton, M.H., Denison, M.S., 2015.
500 Development of Species-Specific Ah Receptor-Responsive Third Generation CALUX
501 Cell Lines with Enhanced Responsiveness and Improved Detection Limits. *Environ. Sci.*
502 *Technol.* 49, 11903–11912. <https://doi.org/10.1021/acs.est.5b02906>
- 503 Dahl, A., Gharibi, A., Swietlicki, E., Gudmundsson, A., Bohgard, M., Ljungman, A.,
504 Blomqvist, G., Gustafsson, M., 2006. Traffic-generated emissions of ultrafine particles

505 from pavement-tire interface. *Atmos. Environ.* 40, 1314–1323.
506 <https://doi.org/10.1016/j.atmosenv.2005.10.029>

507 Degaffe, F.S., Turner, A., 2011. Leaching of zinc from tire wear particles under simulated
508 estuarine conditions. *Chemosphere* 85, 738–743.
509 <https://doi.org/10.1016/j.chemosphere.2011.06.047>

510 Escher, B.I., Neale, P.A., Villeneuve, D.L., 2018. The advantages of linear concentration-
511 response curves for in vitro bioassays with environmental samples. *Environ. Toxicol.*
512 *Chem.* 37, 2273–2280. <https://doi.org/10.1002/etc.4178>

513 Grigoratos, T., Martini, G., 2014. Non-exhaust traffic related emissions. Brake and tyre wear
514 PM, JRC Science and Policy Reports. <https://doi.org/10.2790/21481>

515 Han, Y., Cao, J., Posmentier, E.S., Fung, K., Tian, H., An, Z., 2008. Particulate-associated
516 potentially harmful elements in urban road dusts in Xi'an, China. *Appl. Geochemistry*
517 23, 835–845. <https://doi.org/10.1016/j.apgeochem.2007.09.008>

518 Jahnke, A., Sobek, A., Bergmann, M., Bräunig, J., Landmann, M., Schäfer, S., Escher, B.I.,
519 2018. Emerging investigator series: effect-based characterization of mixtures of
520 environmental pollutants in diverse sediments. *Environ. Sci. Process. Impacts* 20, 1667–
521 1679. <https://doi.org/10.1039/C8EM00401C>

522 Kayhanian, M., McKenzie, E.R., Leatherbarrow, J.E., Young, T.M., 2012. Characteristics of
523 road sediment fractionated particles captured from paved surfaces, surface run-off and
524 detention basins. *Sci. Total Environ.* 439, 172–186.
525 <https://doi.org/10.1016/j.scitotenv.2012.08.077>

526 Kim, G., Lee, S., 2018. Characteristics of Tire Wear Particles Generated by a Tire Simulator
527 under Various Driving Conditions. *Environ. Sci. Technol.* 52, 12153–12161.
528 <https://doi.org/10.1021/acs.est.8b03459>

529 Klöckner, P., Reemtsma, T., Eisentraut, P., Braun, U., Ruhl, A.S., Wagner, S., 2019. Tire and
530 road wear particles in road environment – Quantification and assessment of particle
531 dynamics by Zn determination after density separation. *Chemosphere* 222, 714–721.
532 <https://doi.org/10.1016/j.chemosphere.2019.01.176>

533 Klöckner, P., Seiwert, B., Eisentraut, P., Braun, U., Reemtsma, T., Wagner, S., 2020.
534 Characterization of tire and road wear particles from road runoff indicates highly
535 dynamic particle properties. *Water Res.* 185, 116262.
536 <https://doi.org/10.1016/j.watres.2020.116262>

537 Kloepfer, A., Jekel, M., Reemtsma, T., 2005. Occurrence, sources, and fate of benzothiazoles
538 in municipal wastewater treatment plants. *Environ. Sci. Technol.* 39, 3792–3798.
539 <https://doi.org/10.1021/es048141e>

540 Kole, P.J., Löhr, A.J., Van Belleghem, F., Ragas, A., 2017. Wear and Tear of Tyres: A
541 Stealthy Source of Microplastics in the Environment. *Int. J. Environ. Res. Public Health*
542 14, 1265. <https://doi.org/10.3390/ijerph14101265>

543 König, M., Escher, B.I., Neale, P.A., Krauss, M., Hilscherová, K., Novák, J., Teodorović, I.,
544 Schulze, T., Seidensticker, S., Kamal Hashmi, M.A., Ahlheim, J., Brack, W., 2017.
545 Impact of untreated wastewater on a major European river evaluated with a combination
546 of in vitro bioassays and chemical analysis. *Environ. Pollut.* 220, 1220–1230.
547 <https://doi.org/10.1016/j.envpol.2016.11.011>

548 Kovochich, M., Liong, M., Parker, J.A., Oh, S.C., Lee, J.P., Xi, L., Kreider, M.L., Unice,
549 K.M., 2021. Chemical mapping of tire and road wear particles for single particle
550 analysis. *Sci. Total Environ.* 757, 144085.
551 <https://doi.org/10.1016/j.scitotenv.2020.144085>

552 Kreider, M.L., Panko, J.M., McAtee, B.L., Sweet, L.I., Finley, B.L., 2010. Physical and
553 chemical characterization of tire-related particles: Comparison of particles generated
554 using different methodologies. *Sci. Total Environ.* 408, 652–659.

555 <https://doi.org/10.1016/j.scitotenv.2009.10.016>

556 Mummullage, S., Egodawatta, P., Ayoko, G.A., Goonetilleke, A., 2016. Use of
557 physicochemical signatures to assess the sources of metals in urban road dust. *Sci. Total*
558 *Environ.* 541, 1303–1309. <https://doi.org/10.1016/j.scitotenv.2015.10.032>

559 Neale, P.A., Altenburger, R., Ait-Aïssa, S., Brion, F., Busch, W., de Aragão Umbuzeiro, G.,
560 Denison, M.S., Du Pasquier, D., Hilscherová, K., Hollert, H., Morales, D.A., Novák, J.,
561 Schlichting, R., Seiler, T.-B., Serra, H., Shao, Y., Tindall, A.J., Tollefsen, K.E.,
562 Williams, T.D., Escher, B.I., 2017. Development of a bioanalytical test battery for water
563 quality monitoring: Fingerprinting identified micropollutants and their contribution to
564 effects in surface water. *Water Res.* 123, 734–750.
565 <https://doi.org/10.1016/j.watres.2017.07.016>

566 Neale, P.A., Braun, G., Brack, W., Carmona, E., Gunold, R., König, M., Krauss, M.,
567 Liebmann, L., Liess, M., Link, M., Schäfer, R.B., Schlichting, R., Schreiner, V.C.,
568 Schulze, T., Vormeier, P., Weisner, O., Escher, B.I., 2020. Assessing the Mixture
569 Effects in In Vitro Bioassays of Chemicals Occurring in Small Agricultural Streams
570 during Rain Events. *Environ. Sci. Technol.* 54, 8280–8290.
571 <https://doi.org/10.1021/acs.est.0c02235>

572 Polukarova, M., Markiewicz, A., Björklund, K., Strömvall, A.-M., Galfi, H., Andersson
573 Sköld, Y., Gustafsson, M., Järllskog, I., Aronsson, M., 2020. Organic pollutants, nano-
574 and microparticles in street sweeping road dust and washwater. *Environ. Int.* 135,
575 105337. <https://doi.org/10.1016/j.envint.2019.105337>

576 Seiwert, B., Klöckner, P., Wagner, S., Reemtsma, T., 2020. Source-related smart suspect
577 screening in the aqueous environment: search for tire-derived persistent and mobile trace
578 organic contaminants in surface waters. *Anal. Bioanal. Chem.* 412, 4909–4919.
579 <https://doi.org/10.1007/s00216-020-02653-1>

580 Sommer, F., Dietze, V., Baum, A., Sauer, J., Gilge, S., Maschowski, C., Gieré, R., 2018. Tire
581 abrasion as a major source of microplastics in the environment. *Aerosol Air Qual. Res.*
582 18, 2014–2028. <https://doi.org/10.4209/aaqr.2018.03.0099>

583 Tian, Z., Zhao, H., Peter, K.T., Gonzalez, M., Wetzel, J., Wu, C., Hu, X., Prat, J., Mudrock,
584 E., Hettinger, R., Cortina, A.E., Biswas, R.G., Kock, F.V.C., Soong, R., Jenne, A., Du,
585 B., Hou, F., He, H., Lundeen, R., Gilbreath, A., Sutton, R., Scholz, N.L., Davis, J.W.,
586 Dodd, M.C., Simpson, A., McIntyre, J.K., Kolodziej, E.P., 2020. A ubiquitous tire
587 rubber-derived chemical induces acute mortality in coho salmon. *Science* 5, eabd6951.
588 <https://doi.org/10.1126/science.abd6951>

589 Unice, K.M., Weeber, M.P., Abramson, M.M., Reid, R.C.D., van Gils, J.A.G., Markus, A.A.,
590 Vethaak, A.D., Panko, J.M., 2019a. Characterizing export of land-based microplastics to
591 the estuary - Part I: Application of integrated geospatial microplastic transport models to
592 assess tire and road wear particles in the Seine watershed. *Sci. Total Environ.* 646,
593 1639–1649. <https://doi.org/10.1016/j.scitotenv.2018.07.368>

594 Unice, K. M., Weeber, M.P., Abramson, M.M., Reid, R.C.D., van Gils, J.A.G., Markus,
595 A.A., Vethaak, A.D., Panko, J.M., 2019b. Characterizing export of land-based
596 microplastics to the estuary - Part II: Sensitivity analysis of an integrated geospatial
597 microplastic transport modeling assessment of tire and road wear particles. *Sci. Total*
598 *Environ.* 646, 1650–1659. <https://doi.org/10.1016/j.scitotenv.2018.08.301>

599 Wagner, S., Hüffer, T., Klöckner, P., Wehrhahn, M., Hofmann, T., Reemtsma, T., 2018. Tire
600 wear particles in the aquatic environment - A review on generation, analysis,
601 occurrence, fate and effects. *Water Res.* 139, 83–100.
602 <https://doi.org/10.1016/j.watres.2018.03.051>

603 Wang, C.-F., Chang, C.-Y., Tsai, S.-F., Chiang, H.-L., 2005. Characteristics of Road Dust
604 from Different Sampling Sites in Northern Taiwan. *J. Air Waste Manage. Assoc.* 55,

605 1236–1244. <https://doi.org/10.1080/10473289.2005.10464717>
606 Wang, X.J., Hayes, J.D., Wolf, C.R., 2006. Generation of a Stable Antioxidant Response
607 Element–Driven Reporter Gene Cell Line and Its Use to Show Redox-Dependent
608 Activation of Nrf2 by Cancer Chemotherapeutic Agents. *Cancer Res.* 66, 10983–10994.
609 <https://doi.org/10.1158/0008-5472.CAN-06-2298>
610 Zafra, C.A., Temprano, J., Tejero, I., 2011. Distribution of the concentration of heavy metals
611 associated with the sediment particles accumulated on road surfaces. *Environ. Technol.*
612 32, 997–1008. <https://doi.org/10.1080/09593330.2010.523436>
613 Zanders, J.M., 2005. Road sediment: characterization and implications for the performance of
614 vegetated strips for treating road run-off. *Sci. Total Environ.* 339, 41–47.
615 <https://doi.org/10.1016/j.scitotenv.2004.07.023>
616 Zhang, J., Zhang, X., Wu, L., Wang, T., Zhao, J., Zhang, Y., Men, Z., Mao, H., 2018.
617 Occurrence of benzothiazole and its derivatives in tire wear, road dust, and roadside soil.
618 *Chemosphere* 201, 310–317. <https://doi.org/10.1016/j.chemosphere.2018.03.007>
619